The association for medical ultrasound
aium
AMERICAN INSTITUTE OF ULTRASOUND IN MEDICINE

**Still Time to Attend ONLINE!**

46th Annual

# Advanced OB&GYN Ultrasound Seminar

EARN UP TO 20.5

## Focused on Your Toughest Diagnostic Challenges

**February 15–18, 2023** | **Disney's Yacht and Beach Club Resorts • Lake Buena Vista, Florida**

**Preseminar: February 15: Principles of Sonography and Doppler Ultrasound**

## World-Class Faculty

### Program Leaders

**Alfred Z. Abuhamad**
*MD, FAIUM*
Co-Director

**Beryl Benacerraf**
*MD, FAIUM*
Co-Director in Memoriam

### Founders

**Lennard D. Greenbaum**
*MD, FAIUM*
Director Emeritus

**Frederick W. Kremkau**
*PhD, FAIUM*
Director Emeritus

**Brett D. Einerson**
*MD, MPH*

**Yvette S. Groszmann**
*MD, MPH, FAIUM*

**Lawrence D. Platt**
*MD, FAIUM*

**Elena Sinkovskaya**
*MD, PhD, FAIUM*

**Joanne Stone**
*MD, MS*

## Cutting-edge Sessions & Topics

- Abnormal Uterine Bleeding
- Adnexal Masses
- Complicated Multiple Gestations
- Diagnosing Genetic Syndromes
- Fetal Chest Malformations
- Fetal Growth Restriction
- Imaging of the Fetal Brain
- Imaging of the Fetal Heart
- Pelvic Pain

IN PROUD PARTNERSHIP WITH

ORLANDO HEALTH

Wake Forest® School of Medicine

View full agenda and register at
**aium.org/OBGYNseminar**

# Pulse-Echo Technique to Compensate for Laminate Membrane Transmission Loss in Phantom-Based Ultrasonic Attenuation Coefficient Measurements

*Karthik Nagabhushana, MS, Qiuyu Wang, BS, Aiguo Han, PhD*

*Received October 8, 2021, from the Bioacoustics Research Laboratory, Department of Electrical and Computer Engineering, and National Center for Supercomputing Applications, University of Illinois Urbana-Champaign, Urbana, IL, USA (K.N., A.H.); and Bioacoustics Research Laboratory, Department of Electrical and Computer Engineering, University of Illinois Urbana-Champaign, Urbana, IL, USA (Q.W.). Manuscript accepted for publication April 30, 2022.*

*The authors would like to thank Prof. William D. O'Brien, Jr. for his helpful discussions and edits to the manuscript. This work was supported in part by the National Institutes of Health (R01CA226528, R01DK106419, R01HD089935, and R21EB032638), VA San Diego Healthcare System, and National Center for Supercomputing Applications. The content is solely the responsibility of the authors and does not necessarily represent the official views of the funding agencies. Additionally, this work made use of the Illinois Campus Cluster, a computing resource that is operated by the Illinois Campus Cluster Program (ICCP) in conjunction with the National Center for Supercomputing Applications and that is supported by funds from the University of Illinois at Urbana-Champaign. Portions of this work were presented in International Ultrasonics Symposiums in 2020 and 2021.*

*Address correspondence to Aiguo Han, PhD, Bioacoustics Research Laboratory, Department of Electrical and Computer Engineering, University of Illinois at Urbana-Champaign, 306 N Wright Street, Urbana, IL 61801, USA.*

*E-mail: han51@illinois.edu*

**Abbreviations**

*AC, attenuation coefficient; BSC, backscatter coefficient; PEQUS, pulse-echo quantitative ultrasound; PML, perfectly matched layer; PMW, phantom-membrane-water; PPW, points per wavelength; QUS, quantitative ultrasound; RF, radiofrequency; RMS, root-mean-square; ROI, region of interest; SoS, speed of sound; WMP, water-membrane-phantom*

doi:10.1002/jum.16005



***Objectives***—Accurately measuring the attenuation coefficient (AC) of reference phantoms is critical in clinical applications of quantitative ultrasound. Phantom AC measurement requires proper compensation of membrane transmission loss. Conventional methods require separate membrane samples to obtain membrane transmission loss. Unfortunately, separate membrane samples are often unavailable. A pulse-echo approach is proposed herein to compensate for membrane transmission loss without requiring separate membrane samples.

***Methods***—The proposed method consists of the following steps. First, the insertion loss, caused by phantom attenuation and membrane transmission loss, is measured. Second, the membrane reflection coefficient is measured. Third, the unknown acoustic parameters of the membrane and phantom material are estimated by fitting theoretical reflection coefficient to the measured one. Finally, the fitted parameters are used to estimate membrane transmission loss and phantom AC. The proposed method was validated through k-Wave simulations and phantom experiments. Experimental AC measurements were repeated on 5 distinct phantoms by 2 operators to assess the repeatability and reproducibility of the proposed method. Five transducers were used to cover a broad bandwidth (0.7–16 MHz).

***Results***—The acquired AC in the simulations had a maximum error of 0.06 dB/cm-MHz for simulated phantom AC values ranging from 0.5 to 1 dB/cm-MHz. The acquired AC in the experiments had a maximum error of 0.045 dB/cm-MHz for phantom AC values ranging from 0.28 to 1.48 dB/cm-MHz. Good repeatability and cross-operator reproducibility were observed with a mean coefficient of variation below 0.054.

***Conclusion***—The proposed method simplifies phantom AC measurement while providing satisfactory accuracy and precision.

***Key Words***—attenuation coefficient (AC) measurements; k-Wave simulations; quantitative ultrasound (QUS); reference phantom; transmission loss

Quantitative ultrasound (QUS) is an emerging field in medical ultrasound. While conventional B-mode ultrasonic imaging is qualitative, QUS techniques process the raw radiofrequency (RF) data to extract quantitative image parameters such as attenuation coefficient (AC) and backscatter

 

coefficient (BSC). QUS has been shown effective in numerous preclinical and clinical studies such the liver,[1] kidney,[2] prostate,[3] eyes,[4] and blood.[5] More recent clinical applications include the evaluation of breast cancer response to chemotherapy,[6] diagnosing prostate cancer,[7] and diagnosis and fat-fraction quantification of nonalcoholic fatty liver disease.[8,9] Currently, most QUS applications require the capability to calibrate the clinical scanner's pulse-echo signals. Most commonly, the *reference phantom method*[10] is used, a method that requires a calibrated reference phantom. While a long-term QUS goal is to eliminate the reference phantom method as part of the clinical exam, the field is not there yet, but there has been some progress. One phantom-free convolutional neural network approach has shown success.[11] Additionally, as commercial companies increase the diagnostic capabilities of their ultrasonic imaging systems, there are at least two ultrasound companies that have done so by incorporating into their scanners QUS capabilities to yield on-screen quantitative QUS outcomes as subjects are scanned; one being Siemens (ACUSON Sequoia)[12] using an integrated phantom approach and the other being GE (LOGIC E10)[13] using their ultrasound-guided attenuation parameter (UGAP), both approaches being liver-specific. Note that, as work for phantom-free approaches proceeds, it will still be necessary to have a phantom calibration capability for validation of techniques and/or quality control capabilities of QUS-based ultrasound systems; perhaps some simplified procedures for sonographers to provide periodic and/or spot checks. Thus, there is a significant need to continue to improve the technical capabilities to calibrate phantoms so that fundamental tissue properties like AC and BSC are clinically available.

The reference phantom is generally composed of artificial materials that have similar acoustic properties (AC, BSC, and speed of sound [SoS]) as the tissue under examination. The phantom material is typically housed in a cylindrical supportive casing, with the top–bottom surfaces lined with thin protective membranes for ease of use in clinical environments. The reference phantom must be at least as big as the tissue's region of interest (ROI) as shown in Figure 1. An ROI can be as large as 15 cm × 15 cm × 25 cm (for scanning liver) to as small as 5 cm × 5 cm × 2.5 cm (for scanning rat mammary tumors). Two scans are performed using the *reference phantom method* to obtain tissue AC and BSC, as shown in Figure 1. Scan 1: scanner settings (focusing, gain, transmit power, etc.) are optimized to image the tissue (or organ) of interest. Scan 2: reference phantom is imaged with the same scanner settings as scan 1. The reference phantom's AC, BSC, and SoS are known a priori through an independent calibration.[14,15] Hence, by comparing the RF data between scan 1 and scan 2, the system effects are canceled and the tissue AC and BSC are estimated. Consequently, the tissue AC and BSC accuracies depend on the calibrated reference phantom accuracy. In practice, to account for reference phantom changes, if any, detailed calibrations are performed at regular intervals. Recently, recognizing the potential clinical impact of QUS, the pulse-echo QUS (PEQUS) biomarker committee, under the aegis of AIUM and Quantitative Imaging Biomarker Alliance, has focused on clinical translation of three acoustic biomarkers: AC, BSC, and SoS. Understandably, the committee has emphasized the need to standardize QUS methods (which mostly rely on reference phantoms) while improving their accuracy and precision. Consequently, there is a critical need to calibrate the reference phantom's AC, BSC, and SoS accurately and

**Figure 1.** Reference phantom method to extract spectral QUS parameters (BSC and AC).

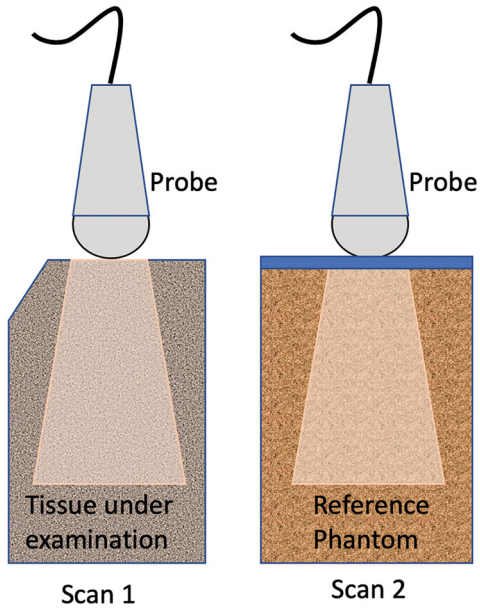

**Figure 2.** Typical QUS reference phantom (side view). Membrane thickness ($L$) is much less than phantom thickness ($H$). All the parameters and their symbols are elaborated in Table 1.

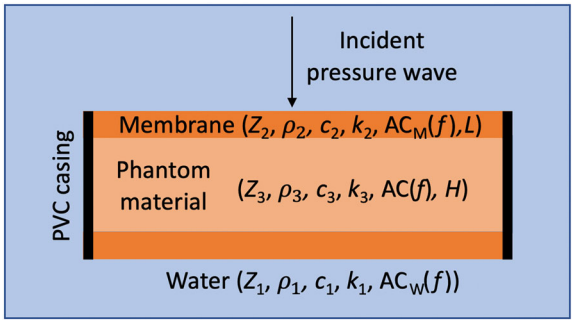


precisely using well-characterized and repeatable methodologies.

Typically, the phantom is immersed in degassed, distilled water during calibration (Figure 2). The top and bottom phantom membranes are assumed to have the same properties (always important to verify with the vendor). The membranes perform the crucial task of isolating the phantom material from external media but also result in a transmission loss of the ultrasonic waves propagating through them. Consequently, measurements of phantom material AC (hereafter referred to as phantom AC) must be corrected for membrane transmission loss. Traditionally, through-transmission techniques have been employed to characterize phantom AC with reasonable accuracy.[15,16] These techniques measure the insertion loss that combines the effects of phantom AC and membrane transmission loss. The techniques require knowledge of membrane transmission loss to derive phantom AC from the insertion-loss measurement.

Conventionally, the membrane transmission loss was approximated by elaborate measurements.[15] These methods require standalone membrane specimens and phantom material that may not be available. To address these issues, a method is proposed herein to directly estimate the membrane transmission loss for a given phantom using a single-element transducer in a pulse-echo configuration.

The proposed technique estimates the phantom AC without requiring additional membrane samples or prior knowledge of the phantom material and membrane properties. While the conventional method estimates the membrane loss of a standalone membrane specimen, the proposed method estimates the membrane loss for the given phantom. Thus, any variation in membrane loss across specimens or within an individual specimen over time can be factored out of phantom AC measurements. Furthermore, this method can be adopted by phantom manufacturers or third-party calibrators as part of their reference phantom calibration strategy that would be necessary for widespread clinical adoption of reference phantom-based QUS applications, as envisioned by the PEQUS biomarker committee.

**Table 1.** Phantom Parameters and Their Symbols

| Parameter | Water | Membrane | Phantom Material | Unit |
|---|---|---|---|---|
| Density | $\rho_1$ | $\rho_2$ | $\rho_3$ | kg/m$^3$ |
| Sound speed | $c_1$ | $c_2$ | $c_3$ | m/s |
| Acoustic impedance | $Z_1$ | $Z_2$ | $Z_3$ | MRayl |
| Wavenumber | $k_1$ | $k_2$ | $k_3$ | m$^{-1}$ |
| Thickness | - | L | H | cm |
| Attenuation coefficient | $AC_W$ | $AC_M$ | AC | dB/cm-MHz |

In this paper, the technique was experimentally evaluated using different phantoms and transducers over a range of frequencies (0.7–16 MHz). The chosen frequency range was relevant in typical QUS applications such as in the characterization of the liver (1–6 MHz),[1,8,9] kidney (5–15 MHz),[2] prostate (4–8 MHz),[3] eyes (5–15 MHz),[4] and blood (9–28 MHz).[17] Additionally, a simulation-based validation of the technique was conducted using k-Wave, a MATLAB toolbox to simulate acoustic wave fields.[18] The k-Wave tool allows users to define the acoustic properties (AC, SoS, and density) of a medium and to customize the transducer (physical shape, transmit pulse, receive characteristics, etc.). Then, k-Wave simulates the acoustic wave fields in the medium and subsequently, the received RF signal. Finally, the proposed technique's robustness and limitations were analyzed based on the experimental and simulation results.

## Materials and Methods

### *Study Design and Participants*

No human or animal studies were conducted.

**Figure 3.** Pulse-echo setups for the proposed technique of measuring phantom AC. The RF data in red represent transmit pulse and the RF data in blue represent the received echoes. The echoes of interest include $E_r$ in setup 1 (**A**) produced by Plexiglas; $E_1$, $E_2$, and $E_3$ in setup 2 (**B**) produced by top-membrane, bottom membrane, and Plexiglas, respectively; and $E_m$ in setup 3 (**C**) produced by top membrane. Their corresponding propagation times are denoted by $t_r$, $t_1$, $t_2$, $t_3$, and $t_m$, respectively. $D$ and transducer diameter values used in this paper are given in Tables 2 and 4; $D$ is three to six times the transducer diameter. The Plexiglas is at least four times wider than the transducer diameter.

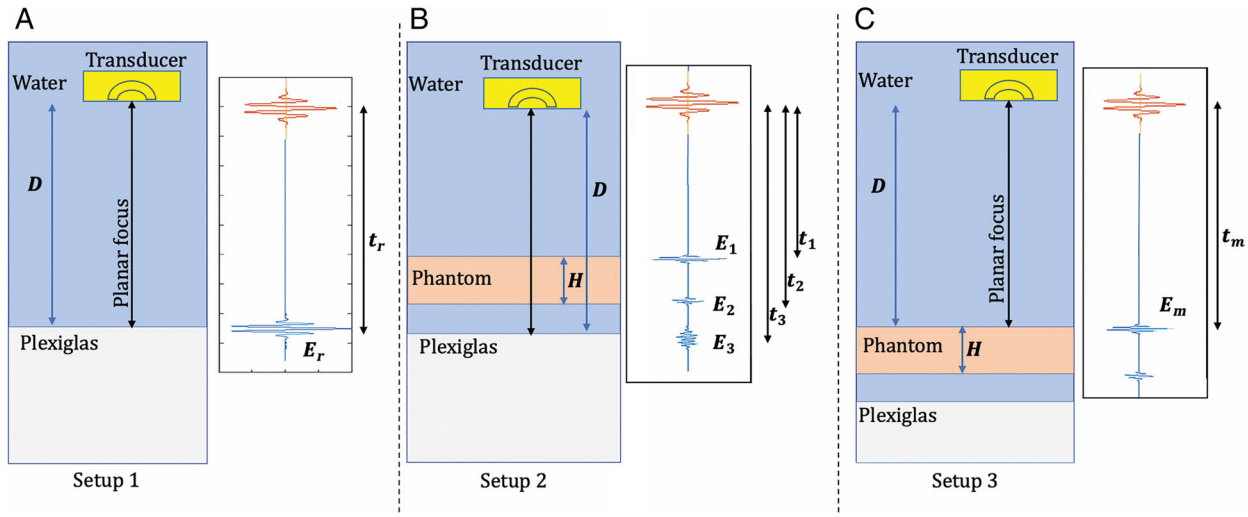


### *Theory*

Consider an ultrasonic plane wave incident normally on a thin membrane (Figure 2). Due to a change in acoustic impedance at the interface, a reflected wave (in the opposite direction of the incident wave) and a transmitted wave (along the direction of the incident wave) are generated. The ratio of the reflected pressure wave to the incident pressure wave is the pressure reflection coefficient. The ratio of the transmitted pressure wave to the incident pressure wave is the pressure transmission coefficient. Let the pressure reflection coefficient for the water-membrane-phantom (WMP) and phantom-membrane-water (PMW) interfaces be $R_1$ and $R_2$, respectively. Similarly, let the pressure transmission coefficients for the WMP and PMW interfaces be $T_1$ and $T_2$, respectively. Like AC and BSC, the reflection coefficients and transmission coefficients are also frequency-dependent. The top and bottom membranes are assumed to be the same and are reasonably assumed to be non-attenuative ($AC_M(f) = 0$). Then, in a pulse-echo setup, the top and bottom membranes cumulatively cause a round-trip transmission coefficient $T_{\text{roundtrip}}(f) = [T_1(f)T_2(f)]^2$ which must be compensated to accurately measure the phantom AC. To compensate for $T_{\text{roundtrip}}$, all the acoustic parameters in Figure 2 must be known or estimated. While $Z_1$ (acoustic impedance of water) can be calculated using the water temperature,[19] other parameters are unknown and must be estimated. In our method, this estimation is done by measuring the magnitude of the WMP

**Figure 4.** Procedure for estimating the magnitude of round-trip transmission coefficient.

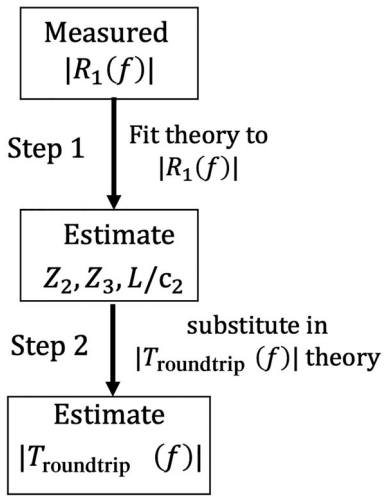

**Table 2.** Properties of Transducers Used in the Phantom AC Measurements

| Transducer ID | Part Number | Center Frequency (MHz) | Pulse Duration (μs) | Diameter (mm) | *F#* | Planar Focus (D) (mm) |
|---|---|---|---|---|---|---|
| TX_1.5M | IL1506HR (Valpey Fisher Inc., Hopkinton, MA) | 1.6 | 2.90 | 19.1 | 4 | 72.4 |
| TX_3.5M | V382 (Panametrics Inc, Waltham, MA) | 3.8 | 0.85 | 12.7 | 4 | 73.8 |
| TX_5M | IL0506HR (Valpey Fisher Inc.) | 5.4 | 0.80 | 19.1 | 3 | 56.9 |
| TX_7.5M | V321 (Panametrics Inc) | 8.1 | 0.38 | 19.1 | 4 | 75.0 |
| TX_10M | IS1004HR (Valpey Fisher Inc) | 12.7 | 0.36 | 12.7 | 4 | 54.4 |

reflection coefficient $|R_1(f)|$ and then fitting the theoretical equation[20] to it. The theory behind this procedure is elaborated in the Appendix.

### *Measurement Steps*

The measurement setup employs a single-element transducer arranged in a pulse-echo configuration (Figure 3). The surface of interest is placed at the planar focus at a distance, $D$, from the transducer for all setups. The planar focus is determined by moving the planar reference surface (Plexiglas in this paper) to maximize the echo amplitude.

#### *Measuring Phantom Insertion Loss*

The phantom insertion loss is measured using setups 1 and 2. First, the reference echo, $E_r$, is acquired from the Plexiglas surface placed at the transducer focus, without phantom insertion (setup 1; Figure 3A). Next, the phantom specimen is inserted between Plexiglas and the transducer (setup 2; Figure 3B) to acquire echoes $E_1$, $E_2$, and $E_3$ (attenuation echo). $E_3$ is used along with $E_r$ to calculate the phantom insertion loss as

$$\text{Insertion loss}(f) = 20\ \log_{10}\left(\frac{|E_r(f)|}{|E_3(f)|}\right). \tag{1}$$

The phantom insertion loss is expressed in terms of the phantom AC and membrane transmission coefficients as

$$\text{Insertion loss}(f) = 2fH[\text{AC}(f) - \text{AC}_W(f)] - 20\log_{10}|T_{\text{roundtrip}}(f)|, \tag{2}$$

where $\text{AC}(f)$ is the frequency-dependent AC (in dB/cm-MHz) of the phantom material, $f$ is the frequency (in MHz), and $H$ is the phantom thickness (in cm). $\text{AC}_W(f)$ is the frequency-dependent AC (in dB/cm-MHz) of the water determined using the temperature ($\tau$, in degree Celsius).[21]

#### *Estimating Round-Trip Membrane Transmission Coefficient*

Membrane echo, $E_m$, is recorded by placing the phantom top surface with the membrane at the planar focus (setup 3; Figure 3C). The magnitude of the WMP reflection coefficient $R_1(f)$ is estimated by

$$|R_1(f)| = |R_{\text{plexi}}| \cdot \frac{|E_m(f)|}{|E_r(f)|}, \tag{3}$$

where the water-Plexiglas reflection coefficient, $R_{\text{plexi}}$, is 0.375 based on the Plexiglas sound speed of 2758 m/s and density of 1180 (kg/m$^3$).[22,23] $|T_{\text{roundtrip}}(f)|$ is then estimated from $|R_1(f)|$ using the procedure shown in Figure 4. Specifically, the theoretical $|R_1(f)|$ equation (see Appendix) is fitted to the measured $|R_1(f)|$ to estimate the unknown parameters $Z_2$, $Z_3$, and $L/c_2$. Finally, the estimated unknown parameters are substituted into the theoretical $|T_{\text{roundtrip}}(f)|$ equation to estimate the roundtrip transmission coefficient. Because multiple solutions can exist in the least square fitting, prior knowledge of phantoms and membranes can be applied to obtain accurate estimates. Generally, the acoustic impedances of membrane and phantom material are greater than water whereby $Z_2$ and $Z_3$ are assumed to lie between 1.5 and 15 MRayl. Furthermore, based on knowledge of the manufacturer's phantom membranes, $L$ ranges between 1 μm and 1 mm, and $c_2$ ranges between 1000 and 5000 m/s. Thus, the ratio $L/c_2$ ranges between 0.2 ns and 1 μs.

Furthermore, ultrasonic waves at the planar focus are assumed to be planar, which is a good approximation

**Figure 5.** k-Wave setups A, B, and C for simulating proposed AC measurement technique (axial cross-section), replicating setups 1, 2, and 3 (in Figure 3), respectively. The transducer position and domain size remained the same for the three setups. The planar focus, at a distance *D* from the transducer, was determined by maximizing the amplitude of the reference echo. PML, perfectly matched layer.

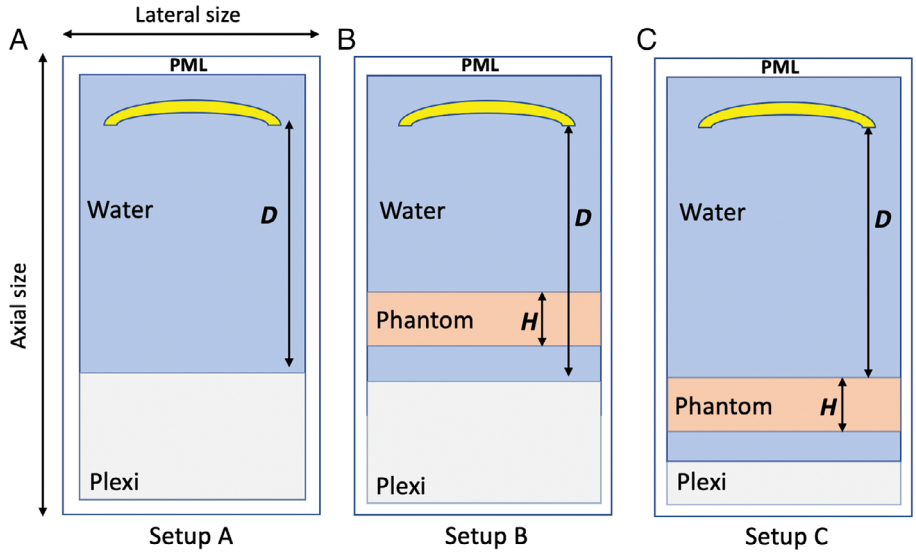


**Table 3.** Material Acoustic Properties in Simulation

| Property | Phantom Material | Membrane | Plexiglas | Water |
|---|---|---|---|---|
| Density (kg/m$^3$) | 1040 | 1690 | 1180 | 1000 |
| Sound speed (m/s) | 1540 | 2400 | 2758 | 1480 |
| Attenuation (dB/cm) | 0.400 $f^{1.3}$ | 0.788 $f^{1.3}$ | 0 | 0.016 $f^{1.3}$ |

**Table 4.** Transducer, Phantom, and Domain Properties Across Simulations

| Property | | Simulation 1 | Simulation 2 |
|---|---|---|---|
| Transducer | Center frequency (MHz) | 10 | 20 |
| | Diameter (mm) | 9.0 | 6.4 |
| | *F#* | 4 | 4 |
| | D (mm) | 36.0 | 25.6 |
| Phantom | Phantom thickness (mm) | 25 | 12 |
| | Membrane thickness (μm) | 63.9 | 64.0 |
| Computational domain | Spatial resolution (μm) | 21.3 | 16.0 |
| | Time step (ns) | 1.93 | 1.45 |

for weakly focused single-element transducers commonly used in QUS applications.[24]

*Estimating Phantom Thickness*

The phantom thickness *H* is estimated by applying a time of flight analysis[15] to the propagation times of the echoes obtained from setups 1 and 2 (see Appendix for a detailed discussion).

*Processing Phantom Attenuation Coefficient*

The estimated round-trip membrane transmission loss and measured phantom thickness are substituted into

**Figure 6.** Measured AC across phantoms and transducers (averaged across operators and individual iterations). For each phantom, multiple curves are present in each frequency range due to measurements from multiple transducers with overlapping bandwidths.

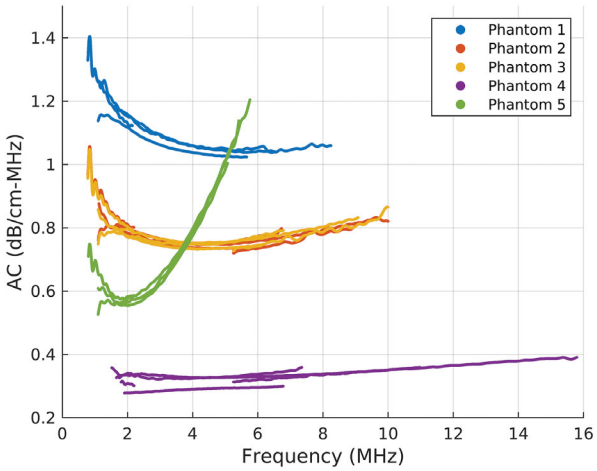


**Figure 7.** Membrane characterization results averaged across operators and individual iterations and compared with the theoretical value.[15] **A**, Measured membrane reflection coefficient (magnitude). **B**, Estimated membrane round-trip transmission coefficient (magnitude).

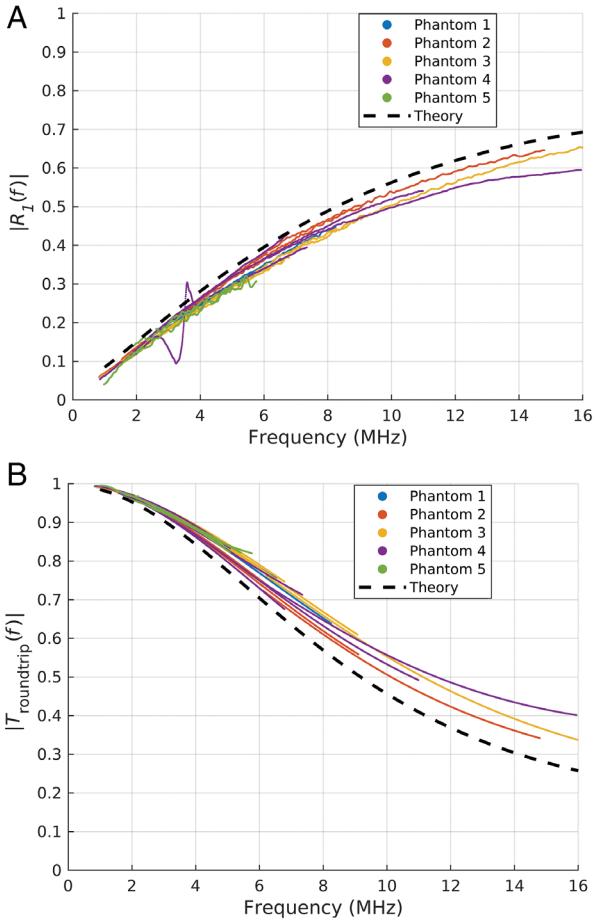


Equations 1 and 2 to estimate the phantom attenuation coefficient, $AC(f)$.

### *Experimental Validation*

AC measurements were performed using conventional methods and methods proposed herein on 5 phantoms with diverse attenuation profiles. The AC results from both methods were compared to validate the proposed method. Furthermore, multiple individual measurements were performed by two different operators to assess the repeatability and cross-operator reproducibility of the measurements.[25]

#### *Setup*

Single-element transducers in a pulse-echo configuration were used for measuring the phantom AC. Plexiglas was used as the planar reference surface. The transducer, phantom, and Plexiglas were immersed in degassed water (Figure 3). The transducer was moved using a motion control system (Daedal Parker Hannifin Corporation, Irwin, PA, USA). The motion control system was preset in such a manner that the transducer's axis was perpendicular to the top surface of Plexiglas. The transducer was connected to a pulser-receiver (UT340, UTEX Scientific Instruments Inc, Mississauga, ON, Canada) followed by a digitizer (PDA14-200 A/D converter, Signatec Inc, Lockport, IL, USA), with a sampling frequency of 200 MHz to digitize the received analog echoes.

#### *Test Conditions*

AC measurements were performed on 5 phantoms, named phantom 1 to phantom 5 (CIRS Inc, Norfolk, VA, USA). The phantoms were made of different tissue-mimicking materials (and hence different AC) but were laminated with the same 25-μm-thick Saran membrane with well-studied properties.[15] While the conventional method incorporated this prior knowledge of the Saran membrane in the AC measurement, the proposed technique estimated the membrane properties for each phantom-transducer combination.

Five weakly focused transducers (Table 2), spanning a frequency range of 0.7 to 16 MHz, were used in the validation. The transducers were excited with a −100 V pulse and the corresponding pulse durations are shown in Table 2. Two operators performed three repeated AC measurements each for all the transducer-phantom combinations. When characterizing with the high-frequency transducer, IS1004HR with a 12.7 MHz center frequency, the attenuation echoes ($E_3$) from phantom 1 and phantom 5 were below the receiver noise floor due to the two phantoms' high attenuation above 10 MHz. Hence, these two transducer-phantom combinations were dropped from the experiment. For each of the remaining transducer-phantom combinations, the intersection of the −20-dB bandwidths of the reference echo and the attenuation echo was chosen as the bandwidth for AC analysis.

*Performance Metrics for the Proposed Method*

The conventional method was used as a reference to quantify the accuracy of the proposed method. Consequently, $\Delta_{AC}$ was calculated for each transducer-phantom combination as

$$\Delta_{AC}(f) = \mu_{AC,P}(f) - \mu_{AC,R}(f), \quad (4)$$

where $\mu_{AC,P}$ and $\mu_{AC,R}$ are AC averaged across iterations and operators for the proposed and reference methods, respectively. Repeatability and cross-operator reproducibility were quantified by calculating the sample standard deviation ($s_{AC}(f)$) across 6 measurements (3 iterations × 2 operators) for each transducer-phantom combination. Furthermore, root-mean-square (RMS) $\Delta_{AC}(f)$ and standard deviation $s_{AC}(f)$ were calculated for each phantom, for all transducers. Also, $s_{AC}(f)$ was normalized by $\mu_{AC,P}$ to calculate the coefficient of variation as

$$\mathrm{cov}_{AC}(f) = \frac{s_{AC}(f)}{\mu_{AC,P}(f)}. \quad (5)$$

***Simulation-Based Validation***

The proposed phantom attenuation measurement technique was applied on a simulated phantom in k-Wave.[18] k-Wave permits programming every aspect of the setup such as phantom acoustic properties and transducer parameters. This simulation-based validation presents 3 significant advantages over experimental validation. First, the phantom AC obtained from the proposed technique can be compared with its ground truth (attenuation profile programmed in k-Wave) for validation. Second, simulation is a cheaper way of validating hypothetical (and potentially useful) phantom-transducer combinations. Finally, k-Wave allows observing the acoustic wave fields created in the medium, permitting the AC measurement technique to be understood at a deeper level, opening avenues for potential improvements. The k-Wave simulation code and the corresponding AC estimation code are made publicly available on GitHub

**Figure 8.** Performance metrics calculated for the proposed method. AC is averaged within a bandwidth of 0.5 MHz, computed across operators and individual iterations (**A**) AC difference compared to the conventional method. **B**, Sample standard deviation of the AC results.

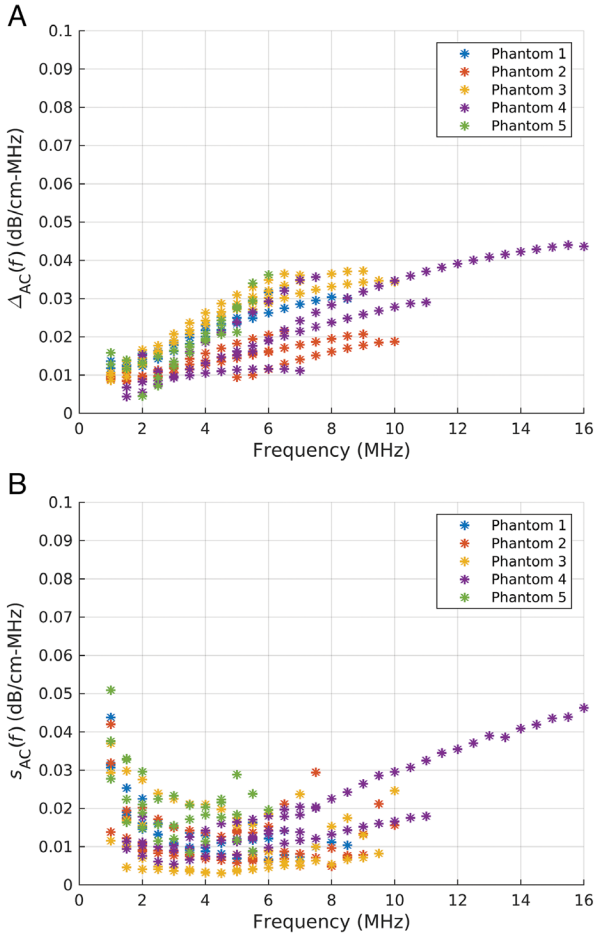

**Table 5.** Performance Metrics of the Proposed Method Across Phantoms

| Phantom | Range of AC($f$) (dB/cm-MHz) | RMS $\Delta_{AC}$ (dB/cm-MHz) | RMS $s_{AC}$ (dB/cm-MHz) | Mean $cov_{AC}$ |
|---|---|---|---|---|
| 1 | 1.021–1.475 | 0.022 | 0.016 | 0.013 |
| 2 | 0.728–1.011 | 0.015 | 0.014 | 0.015 |
| 3 | 0.734–0.976 | 0.027 | 0.014 | 0.015 |
| 4 | 0.281–0.388 | 0.032 | 0.021 | 0.054 |
| 5 | 0.557–1.160 | 0.022 | 0.023 | 0.030 |

(https://github.com/karthiknagabhushana/Phantom-AC-membrane-loss-estimation).

*Setup*

k-Wave simulations were split across 3 setups; each included the transducer, phantom, and Plexiglas (Figure 5). The transmit and receive electromechanical responses were each defined as Gaussian with a fractional bandwidth (−3 dB) of 50%. The k-Wave setup is described in more detail in the Appendix.

*Test Conditions*

Simulations were performed to validate the proposed technique for two phantom-transducer combinations. The acoustic properties of all the materials (Table 3) were kept constant for both simulations. The transducer and phantom properties (Table 4) were chosen to represent typical use scenarios. Accordingly, the properties of the computational domain were chosen to make the simulation computationally tractable while ensuring reasonable accuracy (less than 10% error for the reflection and transmission coefficients; see the Appendix). Finally, the methodological steps enumerated in the Measurement Steps section were simulated in k-Wave for both simulations.

*Performance Metrics*

The predefined phantom AC profile was considered as the reference and $\Delta_{AC}(f)$ was computed (Equation 4) for each simulation to quantify the accuracy. Furthermore, RMS values were computed for $\Delta_{AC}(f)$ for both simulations in their respective bandwidths.

**Figure 9. A**, Acquired AC (with and without membrane $T_{roundtrip}$ compensation) compared with ground truth for simulations 1 and 2. **B**, Difference between acquired AC and the ground truth for simulations 1 and 2.

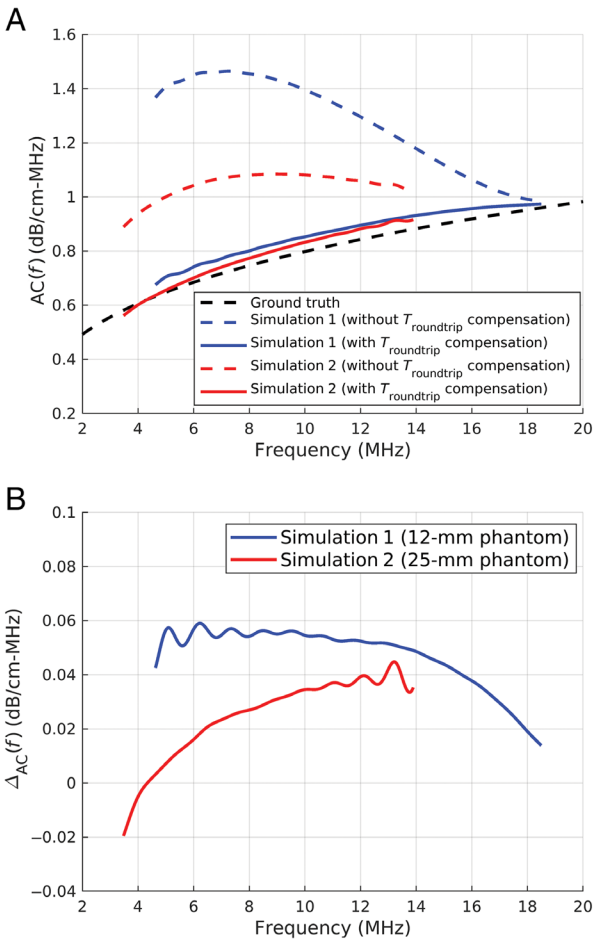


## Results

***Experimental Results***

The measured AC, measured $|R_1(f)|$, and estimated $|T_{roundtrip}(f)|$ for all the phantom-transducer combinations, averaged across operators and individual iterations, are shown in Figures 6 and 7, A and B, respectively. From theory, $|R_1(f)|$ and $|T_{roundtrip}(f)|$ are expected to be periodic and hence will have nulls and peaks in their profile (see the Appendix).

**Figure 10.** **A**, Membrane reflection coefficient (magnitude), acquired from both simulations, compared with ground truth. **B**, Estimated membrane round-trip transmission coefficient (magnitude) compared with ground truth.

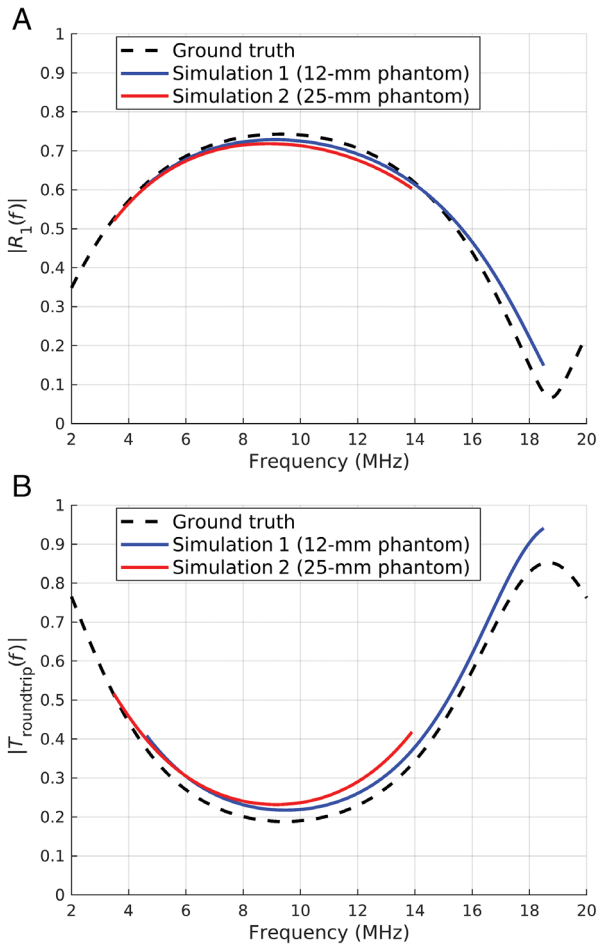


The performance metrics for the proposed method, $\Delta_{AC}(f)$ and $s_{AC}(f)$, are shown in Figure 8, A and B, respectively. Finally, for each phantom, Table 5 listed the RMS $\Delta_{AC}(f)$, the RMS $s_{AC}(f)$, and the mean coefficient of variation, and compared with their respective ACs.

Across all the five phantoms, RMS $\Delta_{AC}$ was 0.025 dB/cm-MHz and RMS $s_{AC}$ was 0.018 dB/cm-MHz. $|T_{roundtrip}(f)|$ varied between 0 and −11.8 dB within a frequency range of 0.7 to 16 MHz and was estimated within 0 to 3.5 dB error. The maximum error occurred at the null of the membrane transmission coefficient.

### *Simulation Results*

The acquired AC and corresponding accuracy metric, $\Delta_{AC}$, are shown for both simulations in Figure 9, A and B, respectively. The acquired $|R_1(f)|$ and the estimated $|T_{roundtrip}(f)|$ are shown for both simulations in Figure 10, A and B, respectively.

The RMS $\Delta_{AC}$ were 0.029 and 0.049 dB/cm-MHz for the 25 and 12-mm phantoms, respectively. $|T_{roundtrip}(f)|$ varied between 0 and −14.5 dB within a frequency range of 3.5 to 18.5 MHz and was estimated within 0 to 2 dB error. The maximum error occurred at the peaks and nulls of the membrane transmission coefficient.

For $|T_{roundtrip}(f)|$, an error of 3.5 dB in the experiments and an error of 2 dB in the simulations must be put in perspective. The errors occur only in a small portion of the bandwidth near the nulls and peaks of the periodic $|T_{roundtrip}(f)|$ and hence do not translate to a large RMS $\Delta_{AC}$. For QUS outcomes, RMS $\Delta_{AC}$ is a more important metric because it captures the aggregate accuracy of the estimated AC over a bandwidth. In contrast, if the membrane loss were not compensated, the AC error is spread over the entire bandwidth as illustrated in Figure 9A for the simulations. Without membrane loss compensation, the RMS $\Delta_{AC}$ for the 25 and 12-mm phantoms was 0.30 and 0.52, respectively, which is nearly 10 times the RMS $\Delta_{AC}$ of our proposed method. This has added significance when we consider that there was no method to measure and compensate membrane loss till now if independent membrane and phantom samples were unavailable.

## Discussion

QUS imaging with reference phantoms has many diagnostic benefits and hence will become more common in the future. The accuracy of the QUS measurements depends on the reference phantom calibration for which we proposed an alternate calibration method that is more amenable to widespread adoption. Although the calibration will be performed regularly by trained individuals, it is valuable for the sonographers to understand the entire workflow to get reliable QUS estimates and clinical inferences. This is particularly germane because QUS capabilities

are already appearing on selected commercial ultrasonic imaging systems with the likelihood that in the near future such capabilities will be ubiquitous in the clinical practice of diagnostic ultrasound.

### *Experimental Validation*

The proposed method successfully measured phantom ACs with diverse attenuation profiles. The laboratory experiments compared the proposed AC measurement technique with the conventional technique and evaluated its accuracy across transducers and phantom attenuation profiles. While the phantoms' AC varied between 0.28 and 1.48 dB/cm-MHz over 0.7 to 16 MHz, the proposed AC method had a maximum error of only 0.045 dB/cm-MHz (see Figure 8A) relative to the conventional method. For a given phantom, there was continuity in the measured AC($f$) for two transducers with overlapping bandwidths. Also, the method was accurate for weakly focused transducers, typically used in QUS applications, with F# between 3 and 4. Finally, the proposed method showed good repeatability and cross-operator reproducibility, with a mean coefficient of variation between 0.013 and 0.054.

### *Simulation-Based Validation*

The proposed method was evaluated by k-Wave simulations, by implementing two hypothetical transducer-phantom combinations. In simulation 1, a 12-mm phantom AC that ranged from 0.5 to 0.9 dB/cm-MHz over 4.6 to 18.5 MHz was successfully measured with a maximum error of 0.060 dB/cm-MHz. In simulation 2, a 25-mm phantom AC that ranged from 0.6 to 1.0 dB/cm-MHz over 3.5 to 13.9 MHz range was successfully measured with a maximum error of 0.045 dB/cm-MHz. AC acquired without membrane transmission loss compensation was plotted (Figure 9A) for both simulations to illustrate the importance of accounting for membrane effects in the AC measurement. Without membrane loss compensation, simulations 1 and 2 had a maximum $\Delta_{AC}$ of 0.76 and 0.36 dB/cm-MHz, respectively, which is significant compared to ground truth AC in the same bandwidth.

Also, the phantom insertion could have changed the diffraction pattern between setups 1 and 2 of Figure 3, potentially introducing diffraction artifacts while calculating the insertion loss. However, this change was found to be negligible in simulations because the sound speed of the reference phantom material is close to that of water.

### *Possible Improvements to the Membrane Estimation Algorithm*

The membrane transmission coefficient's accuracy was estimated experimentally and in simulation (Figures 7B and 10B, respectively). The error in the estimated $|T_{\text{roundtrip}}(f)|$ emerged from the acquired $|R_1(f)|$ that showed a discrepancy in the amplitude and position of nulls and peaks. This discrepancy is possibly due to nonplanar wavefronts at the focus of transducers used in this study, thus violating the plane wave assumption. Diffraction correction can be applied to compensate for the error in estimated $|T_{\text{roundtrip}}(f)|$. Currently, the main source of error in determining AC is the membrane estimation step. For instance, an error of 2 dB in estimated $20\log_{10}|T_{\text{roundtrip}}|$ at 10 MHz would lead to a $\Delta_{AC}$ of 0.04 dB/cm-MHz for a 25-mm phantom (Equation 2). These values closely match the observed error in estimated $|T_{\text{roundtrip}}|$ and $\Delta_{AC}$ for Simulation 1 at 10 MHz (Figures 9B and 10B, respectively). For the same reason, $\Delta_{AC}$ for the thinner phantoms (eg, 12-mm phantom) is greater than the $\Delta_{AC}$ of the thicker phantoms (eg, 25-mm phantom). Hence, the improvement in membrane estimation will further improve the AC measurement technique. Alternatively, as the phantom thickness increases, the accuracy increases for the proposed AC measurement technique.

The membrane is assumed to be nonattenuative in the estimation procedure. This assumption is reasonable in typical scenarios because the cumulative attenuation caused by a thin membrane, $AC_M(f)fL$, is much less than $20\log_{10}|T_{\text{roundtrip}}(f)|$. However, this assumption can fail if the membrane is thick, or highly attenuative, or both. In such cases, membrane attenuation can be incorporated in the reflection and transmission coefficients by representing the membrane wavenumber ($k_2$) as a complex number

$$k_2 = \frac{2\pi f}{c_2} - j\alpha_M(f), \tag{6}$$

where $\alpha_M(f)$ is the frequency-dependent AC (in Np/m) of the membrane.[15] Then, the estimation

procedure would also estimate $\alpha_M(f)$ along with $Z_2$, $Z_3$, and $L/c_2$.

## Conclusion

A simple technique to simultaneously measure laminate membrane transmission loss and the phantom AC has been validated through simulation and laboratory experiments. The technique was validated to be accurate across transducers and phantom thicknesses. Additionally, the technique was repeatable and cross-operator reproducible in laboratory experiments.

## APPENDIX

## Theory

The ultrasonic pressure reflection and transmission coefficients of a thin membrane at normal incidence (Figure 1) are well understood.[20] The pressure reflection and transmission coefficients for the WMP and PMW interfaces are given by

$$R_1(f)=\frac{(Z_3-Z_1)Z_2\cos(k_2L)+j\left(Z_2^2-Z_3Z_1\right)\sin(k_2L)}{(Z_3+Z_1)Z_2\cos(k_2L)+j\left(Z_2^2+Z_3Z_1\right)\sin(k_2L)} \tag{A1}$$

$$R_2(f)=\frac{(Z_1-Z_3)Z_2\cos(k_2L)+j\left(Z_2^2-Z_1Z_3\right)\sin(k_2L)}{(Z_1+Z_3)Z_2\cos(k_2L)+j\left(Z_2^2+Z_1Z_3\right)\sin(k_2L)} \tag{A2}$$

$$T_1(f)=\frac{2Z_3Z_2}{(Z_3+Z_1)Z_2\cos(k_2L)+j\left(Z_2^2+Z_3Z_1\right)\sin(k_2L)} \tag{A3}$$

$$T_2(f)=\frac{2Z_1Z_2}{(Z_1+Z_3)Z_2\cos(k_2L)+j\left(Z_2^2+Z_1Z_3\right)\sin(k_2L)} \tag{A4}$$

The membrane is assumed to be nonattenuative ($AC_M(f)=0$) and hence the wavenumber ($k_2=2\pi f/c_2$) is a real number.

## Measurement Steps

***Measuring Phantom Insertion Loss***

$AC_w(f)$ is the frequency-dependent AC (in dB/cm-MHz) of the water determined using the temperature ($\tau$, in degree Celsius) as[21]

$$AC_w(f)=\left(1-3.84\times10^{-4}\right)\cdot\left(55.9-2.37\tau+4.77\times10^{-2}\tau^2-3.48\times10^{-4}\tau^3\right)\cdot10^{-5}\cdot\left(20\log_{10}e\right)\cdot f^2 \tag{A5}$$

***Measuring Phantom Thickness***

The phantom thickness $H$ is estimated by using the echoes obtained from setups 1 and 2. A time of flight analysis yields

$$H=\frac{c_1}{2}\cdot\left((t_r-t_3)-(t_r-t_2)+(t_r-t_1)\right), \tag{A6}$$

where the sound speed in water, $c_1$, is known, and the time differences $t_r-t_3$, $t_r-t_2$, and $t_r-t_1$ are obtained from the RF data of echoes using cross-correlation. In this method, the phase differences between the echoes can cause an error in the measured thickness up to half a wavelength. However, this is much smaller than the overall phantom thickness and hence can be ignored.

***Processing Phantom Attenuation Coefficient***

The estimated round-trip membrane transmission loss and measured phantom thickness are substituted into Equations 1 and 2 to estimate the phantom attenuation coefficient, $AC(f)$, by

$$AC(f)=AC_w(f)+\frac{1}{2fH}\text{Insertion loss}+\frac{1}{2fH}20\log_{10}\left|T_{\text{roundtrip}}(f)\right| \tag{A7}$$

## Simulation-Based validation

***Setup Details***

The 3-dimensional kspaceFirstOrder3D function in the k-Wave toolbox was utilized to simulate linear ultrasonic wave propagation. Nonlinearity in the

media was ignored to simplify the analysis. The grid spacing was chosen as low as possible based on available computational resources while satisfying the Nyquist criterion. k-Wave requires the attenuation exponent to be homogenous across the computational domain, where the acoustic propagation is simulated.[26] To address this constraint, the same attenuation exponent of the phantom material was assigned to the entire domain. Consequently, a best-fit analysis was performed on the desired attenuation coefficients of water and membrane over the 2 to 30 MHz frequency range to match the attenuation exponent of the phantom. The transducer was simulated by defining points in the 3-dimensional medium along the contour of the spherically focused transducer. The source points were modeled as additive mass sources.[27] The Courant–Friedrichs–Lewy ratio was set to 0.25 to meet the stability conditions for simulating heterogeneous mediums as per the k-Wave manual.[28] A perfectly matched layer (PML) of 20 grid points was used at the boundaries to carry out free-space simulations in a finite computational domain. For perpendicular incidence, a 20-grid-point PML provided a transmission coefficient of −70 dB and a reflection coefficient of −100 dB in the bandwidth of interest (points per wavelength [PPW] >3).[29] Also, to avoid spatial aliasing in the computation domain, high-frequency components in the excitation signal were filtered out using a Kaiser-window-based finite impulse response filter. The filter's corner frequency was chosen based on the spatial resolution and satisfied PPW = 3.

## Quantifying the Accuracy of k-Wave Simulations

For a given grid spacing, the accuracy of k-Wave simulations with heterogeneous media reduces with an increase in ultrasonic frequency.[29] To quantify this effect, additional simulations were run while keeping the grid spacing constant. In these simulations, a broadband plane wave was normally incident onto the Plexiglas and membrane surfaces, and the corresponding frequency-dependent pressure reflection and transmission coefficients were computed by recording the resulting ultrasonic waves. The simulated coefficients were compared with their true values, as programmed in the simulation, to yield an error estimate. Frequency-dependent simulated error estimates of $|R_1(f)|$ and $|T_{\text{roundtrip}}(f)|$ are expressed in PPW (Figure A1, A and B, respectively).

**Figure A1.** Error in modeling water-Plexiglas and WMP surfaces for grid spacings of 16.0 and 21.3 μm across frequency (expressed in points per wavelength). **A**, Pressure reflection coefficient error, and **B**, pressure transmission coefficient error.

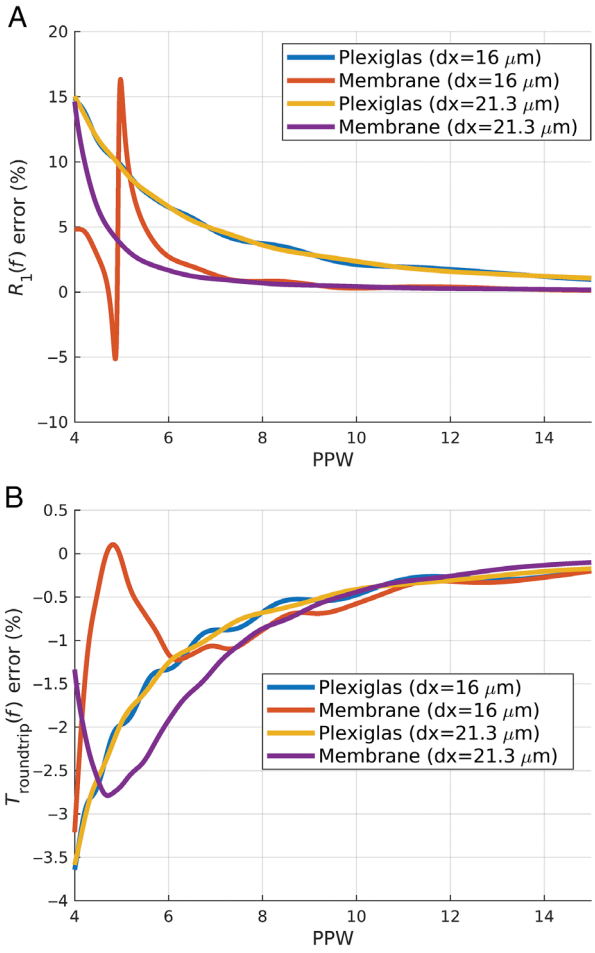


An error threshold of ±10% on the reflection coefficient and a ±3% on the transmission coefficient were adopted for both surfaces leading to a frequency threshold of 5 PPW. This frequency threshold corresponds to an upper threshold of 18.5 MHz for a spatial resolution of 16.0 μm (used with the 20-MHz transducer) and 13.9 MHz for 21.3 μm (used with the 10-MHz transducer). Moreover, since this test quantifies all errors arising from simulating a thin membrane interface, the inaccuracies arising from the

discretization of the 64-μm membrane are also accounted for.

## References


1. Garra BS, Insana MF, Shawker TH, et al. Quantitative ultrasonic detection and classification of diffuse liver disease. Comparison with human observer performance. *Invest Radiol* 1989; 24:196–203.
2. Insana MF, Hall TJ, Wood JG, et al. Renal ultrasound using parametric imaging techniques to detect changes in microstructure and function. *Invest Radiol* 1993; 28:720–725.
3. Feleppa EJ, Kalisz A, Sokil-Melgar JB, et al. Typing of prostate tissue by ultrasonic spectrum analysis. *IEEE Trans Ultrason Ferroelectr Freq Control* 1999; 43:609–619.
4. Feleppa EJ, Lizzi FL, Coleman DJ, et al. Diagnostic spectrum analysis in ophthalmology: a physical perspective. *Ultrasound Med Biol* 1986; 12:623–631.
5. Savery D, Cloutier G. A point process approach to assess the frequency dependence of ultrasound backscattering by aggregating red blood cells. *J Acoust Soc Am* 2001; 110:3252–3262.
6. Sannachi L, Tadayyon H, Sadeghi-Naini A, et al. Non-invasive evaluation of breast cancer response to chemotherapy using quantitative ultrasonic backscatter parameters. *Med Image Anal* 2015; 20:224–236.
7. Rohrbach D, Wodlinger B, Wen J, Mamou J, Feleppa E. High-frequency quantitative ultrasound for imaging prostate cancer using a novel micro-ultrasound scanner. *Ultrasound Med Biol* 2018; 44:1341–1354.
8. Lin SC, Heba E, Wolfson T, et al. Noninvasive diagnosis of nonalcoholic fatty liver disease and quantification of liver fat using a new quantitative ultrasound technique. *Clin Gastroenterol Hepatol* 2015; 13:1337–1345.
9. Han A, Zhang YN, Boehringer AS, et al. Assessment of hepatic steatosis in nonalcoholic fatty liver disease by using quantitative US. *Radiology* 2020; 295:106–113.
10. Yao LX, Zagzebski JA, Madsen EL. Backscatter coefficient measurements using a reference phantom to extract depth-dependent instrumentation factors. *Ultrason Imaging* 1990; 12:58–70.
11. Han A, Byra M, Heba E, et al. Noninvasive diagnosis of nonalcoholic fatty liver disease and quantification of liver fat with radiofrequency ultrasound data using one-dimensional convolutional neural networks. *Radiology* 2020; 295:342–350.
12. Labyed Y, Milkowski A. Novel method for ultrasound-derived fat fraction using an integrated phantom. *J Ultrasound Med* 2020; 39: 2427–2438.
13. Bende F, Sporea I, Şirli R, et al. Ultrasound-guided attenuation parameter (UGAP) for the quantification of liver steatosis using the controlled attenuation parameter (CAP) as the reference method. *Med Ultrason* 2021; 23:7–14.
14. Chen X, Phillips D, Schwarz KQ, Mottley JG, Parker KJ. The measurement of backscatter coefficient from a broadband pulse-echo system: a new formulation. *IEEE Trans Ultrason Ferroelectr Freq Control* 1997; 44:515–525.
15. Wear KA, Stiles TA, Frank GR, et al. Interlaboratory comparison of ultrasonic backscatter coefficient measurements from 2 to 9 MHz. *J Ultrasound Med* 2005; 24:1235–1250.
16. Han A, Andre MP, Erdman JW, et al. Repeatability and reproducibility of a clinically based QUS phantom study and methodologies. *IEEE Trans Ultrason Ferroelectr Freq Control* 2017; 64:218–231.
17. Yu FT, Franceschini E, Chayer B, et al. Ultrasonic parametric imaging of erythrocyte aggregation using the structure factor size estimator. *Biorheology* 2009; 46:343–363.
18. Treeby BE, Cox BT. K-wave: MATLAB toolbox for the simulation and reconstruction of photoacoustic wave fields. *J Biomed Opt* 2010; 15:021314.
19. Lubbers J, Graaff R. A simple and accurate formula for the sound velocity in water. *Ultrasound Med Biol* 1998; 24:1065–1068.
20. Kinsler LE, Frey AR, Coppens AB, Sanders JV. *Fundamentals of Acoustics*. 4th ed. New York, NY: Wiley; 2000.
21. Fisher FH, Simmons VP. Sound absorption in seawater. *J Acoust Soc Am* 1977; 62:558–564.
22. Kuo IY, Hete B, Shung KK. A novel method for the measurement of acoustic speed. *J Acoust Soc Am* 1990; 88:1679–1682.
23. Plexiglas® general information and physical properties. Altuglas International website. https://www.plexiglas.com/export/sites/plexiglas/.content/medias/downloads/sheet-docs/plexiglas-general-information-and-physical-properties.pdf. Accessed April 7, 2021.
24. Oelze ML, Mamou J. Review of quantitative ultrasound: envelope statistics and backscatter coefficient imaging and contributions to diagnostic ultrasound. *IEEE Trans Ultrason Ferroelectr Freq Control* 2016; 63:336–351.
25. Sullivan DC, Obuchowski NA, Kessler LG, et al. Metrology standards for quantitative imaging biomarkers. *Radiology* 2015; 277:813–825.
26. Treeby BE, Jaros J, Rendell AP, et al. Modeling nonlinear ultrasound propagation in heterogeneous media with power law absorption using a k-space pseudospectral method. *J Acoust Soc Am* 2012; 131:4324–4336.
27. Martin E, Ling YT, Treeby BE. Simulating focused ultrasound transducers using discrete sources on regular Cartesian grids. *IEEE Trans Ultrason Ferroelectr Freq Control* 2016; 63:1535–1542.
28. k-Wave User Manual (version 1.1). k-Wave website. http://www.k-wave.org/manual/kwave_user_manual_1.1.pdf. Accessed June 1, 2020.
29. Robertson JL, Cox BT, Jaros J, et al. Accurate simulation of transcranial ultrasound propagation for ultrasonic neuromodulation and stimulation. *J Acoust Soc Am* 2017; 141:1726–1738.